Solar Phys (2021) 296:52
https://doi.org/10.1007/s11207-021-01794-5

The *Fengyun*-3E/*Joint Total Solar Irradiance Absolute Radiometer*: Instrument Design, Characterization, and Calibration

Baoqi Song[1,2] · Xin Ye[1] · Wolfgang Finsterle[3] · Manfred Gyo[3] · Matthias Gander[3] · Alberto Remesal Oliva[3] · Daniel Pfiffner[3] · Yan Zhao[4] · Wei Fang[1]

Received: 29 October 2020 / Accepted: 23 February 2021 / Published online: 22 March 2021
© The Author(s), under exclusive licence to Springer Nature B.V. 2021

Abstract The *Joint Total Solar Irradiance Monitor* (JTSIM) is due to fly onboard the *Fengyun*-3E spacecraft and aims to measure the Total Solar Irradiance (TSI) in orbit. The instruments on the *Fengyun*-3E/JTSIM include the *Digital Absolute Radiometer* (DARA) from the Physikalisch Meteorologisches Observatorium, Davos and World Radiation Center (PMOD/WRC) and the *Solar Irradiance Absolute Radiometer* (SIAR) from the Changchun Institute of Optics, Fine Mechanics and Physics Chinese Academy of Sciences (CIOMP/CAS). Radiometers from Switzerland and China will monitor the TSI variability on the same pointing system for eight years. The scientific data from JTSIM will support the analysis of potential long-term trends in the Sun's variability. In this article, we describe the sensor box and the electronics box of JTSIM, the measurement principle, and the operation mode of SIAR. Before launch, we accomplished some primary calibrations of SIAR in the CIOMP laboratory, including the aperture area, cavity absorption, non-equivalence, diffraction, etc. Other parameters will be calibrated on orbit. The combined uncertainty of SIAR for characterization is 231 – 233 ppm depending on the measurement channel. The characterization of SIAR is an International System of Units (SI)-native scale calibration. An end-to-end calibration against the World Radiometric Reference (WRR) standard or the Total Irradiance Radiometer Facility (TRF) is a procedure where SIAR is directly calibrated with the WRR reference radiometers. The WRR factor for SIAR is 0.99939 – 1.00092 and the combined measurement uncertainty is 0.074% – 0.099%, depending on the measurement channel.

Keywords Instrumentation · Radiometers · Total solar irradiance · Solar radiometry

✉ B. Song
songbaoqipku04@126.com

1 Changchun Institute of Optics, Fine Mechanics and Physics, Chinese Academy of Sciences, 3888 Dongnanhu Road, Changchun, 100033, China

2 University of Chinese Academy of Sciences, Beijing, 100049, China

3 PMOD/WRC, Dorfstrasse 33, 7260 Davos Dorf, Switzerland

4 Jilin University, 2699 Qianjin Street, Changchun, 100033, China

1. Introduction

Total Solar Irradiance (TSI) is an important parameter for the Earth's climate system. The incoming and outgoing electromagnetic radiation determine the Earth's energy balance. Therefore, reliable and continuous monitoring and knowledge of the absolute TSI-value are crucial for understanding, reconstructing, and eventually forecasting the climate on earth.

The determination of TSI has not been an easy task in the past. Spacecraft-based TSI measurements started being recorded from the late 1970s. Radiometers of different measurement principles were sent into space and contributed to the 35 years of TSI records. Many publications have discussed the TSI data record (Kopp, Lawrence, and Rottman, 2005; Thuillier, Dewitte, and Schmutz, 2006; Kopp and Lean, 2011; Schmutz et al., 2013; Yeo, Krivova, and Solanki, 2014; Zacharias, 2014; Walter et al., 2017).

The *Joint Total Solar Irradiance Monitor* (JTSIM) is the new generation of TSI-monitoring instruments, built by the Changchun Institute of Optics, Fine Mechanics and Physics Chinese Academy of Sciences (CIOMP/CAS) in Changchun, China, with the aim of long-term monitoring of TSI in space. JTSIM will be one of the payloads on the Chinese *Fengyun*-3E spacecraft. The *Fengyun* program develops a Chinese meteorological-series spacecraft supported by the National Satellite Meteorological Center (NSMC), China.

JTSIM includes the *Digital Absolute Radiometer* (DARA), from the PMOD/WRC in Davos, Switzerland, and the *Solar Irradiance Absolute Radiometer* (SIAR), from CIOMP/CAS. SIAR and DARA will also be mounted on the same pointing system. DARA is the result of the latest radiometer developments at PMOD/WRC and comprises several innovations compared to the previous generation of PMO6-type radiometers (Brusa and Fröhlich, 1986). SIAR is based on the principle of an electrically calibrated differential heat-flux transducer with a cavity for the efficient absorption of the radiation to be measured. To compensate for temperature drift, SIAR designates one radiometer as the reference radiometer (Fang, 2003; Wang et al., 2007).

CIOMP/CAS has a wealth of experience in building radiometers to measure TSI. Starting in 2002, a new prototype for spacecraft-based measurements, the *Solar Irradiance Monitor* (SIM), was developed by CIOMP. As a result of its low mass and dimensions, it is easier to accommodate onboard spacecraft. In 2002, sponsored by the Chinese Space Program, the *Solar Constant Monitor* (SCM), which was one of 44 scientific payloads of the *Shenzhou*-3 spacecraft, was launched for a test-flight mission. During the five-month mission, the SCM acquired valid solar irradiance data. Based on the SCM, the *Solar Irradiance Monitor*-I (SIM-I) was developed. In 2008, SIM-I was launched as a payload of the *Fengyun*-3A spacecraft, which was the first time that our instrument worked on a meteorological spacecraft in long-term service. SIM-I was aimed at observing solar incident energy, capturing its daily changes and building a climate dataset. In 2010, another SIM-I was launched with the *Fengyun*-3B spacecraft. In 2013, CIOMP developed the SIM-II for space applications. There were some new features of SIM-II, such as the high-precision temperature-control system and the solar tracking system. As a result of these features, the uncertainty of measurement was further reduced relative to SIM-I (Fang et al., 2009; Yang et al., 2013; Wang et al., 2017).

As can be seen in Figure 1, for a long time, the spacecraft data from different instruments have not been consistent with each other with respect to the absolute TSI-value. The absolute TSI-value difference between the *Differential Absolute Radiometer* (DIARAD), which is part of the *Variability of solar IRradiance and Gravity Oscillations* (VIRGO) experiment, the *Total Irradiance Monitor* (TIM) instrument onboard *the SOlar Radiation and Climate Experiment* (SORCE) mission, and *Fengyun-3C*/SIM-II is about 0.35 (Butler et al., 2008;

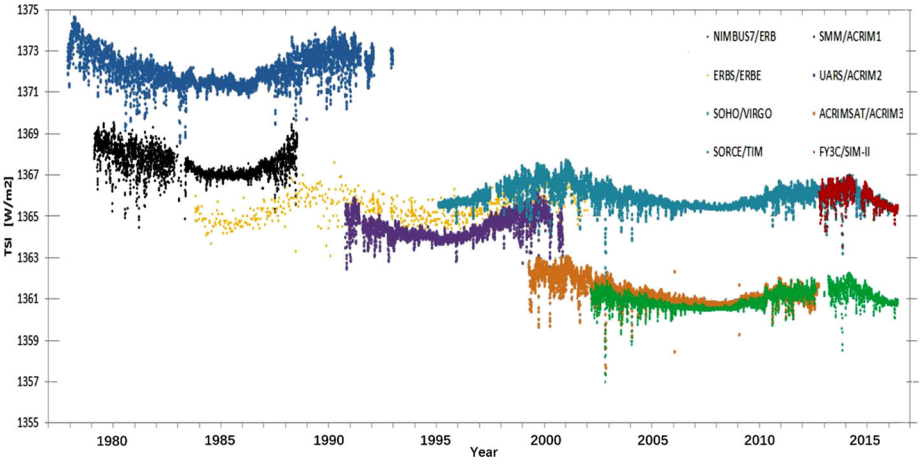

Figure 1 The spacecraft data from different experiments until 2017.

Kopp and Lean, 2011). JTSIM is the first international-cooperation solar-monitor instrument on a Fengyun-series spacecraft. The two instruments will be mounted on the same tracking system and measure solar irradiance at the same time in orbit.

The ultimate goal of JTSIM is to minimize, or correct for, instrumental effects and reduce the measurement uncertainty. The basic radiometer properties, such as the aperture area, cavity absorptance, non-equivalence, and diffraction, can be calibrated at a component level, traceable to the International System of Units (SI), or at a system level by end-to-end calibration against the WRR standard. (The non-equivalence effect is caused by the slight heat-flow difference in the thermal configuration of the active cavity in the measurement and calibration phases.) In this article, we present both the instrument characterization result and the WRR calibration result. In Section 2, the sensor box and the electronics box of the JTSIM instrument are presented. The implementation of the native scale determined from the instrument characterization of JTSIM is presented in Section 3. The results of the JTSIM end-to-end calibration against the WRR standard are introduced in Section 4.

2. Instrument Description

2.1. General Introduction of JTSIM

As can be seen in Figure 2, the instruments on *Fengyun-3E*/JTSIM include the tracking system, DARA, and SIAR. SIAR consists of the sensor box (SB) and the electronics box (EB), which are separated and connected by cables. Three electrical substitution radiometers (Channel 1, Channel 2, and Channel 3) are aligned in a row. Channel 1 is to be used for daily measurements of TSI, while Channel 2 and Channel 3 are to be used occasionally for the degradation investigation of Channel 1. The three radiometers can perform independent measurements or simultaneous measurements by uploaded commands.

SIAR is based on the previous generation of *Fengyun*-3C/SIM-II. The measurement principle is based on an electrically calibrated differential heat-flux transducer with a cavity for the efficient absorption of the radiation to be measured. All cavities of SIAR are equipped with an electrical heater and an absorptive coating for solar radiation.

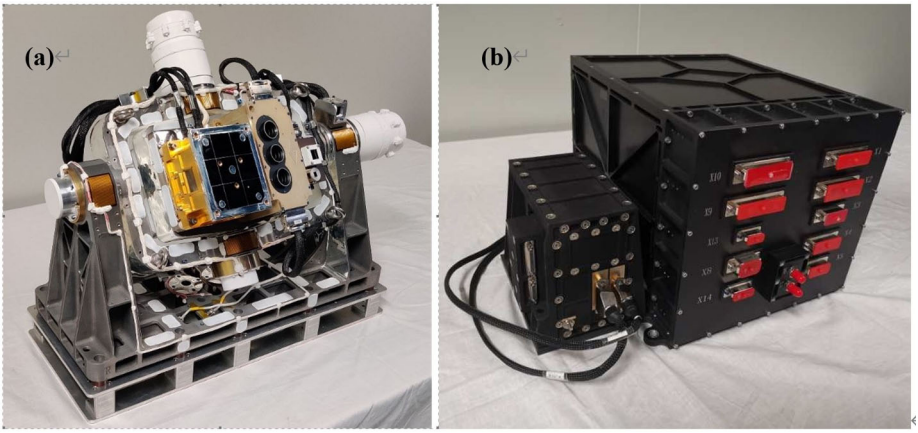

Figure 2 The JTSIM/*Fengyun*-3E Flight Model Instrument: (**a**) sensor box [size: 745 mm× 488 mm × 408 mm], (**b**) electronics box [size: 330 mm × 393 mm × 235 mm].

Table 1 Instrument parameters of *Fengyun*-3E/*Joint Total Solar Irradiance Monitor* (JTSIM).

Parameters	Temp. control accuracy of heat sink	Tracking accuracy of Sun sensor	Size of JTSIM [mm^3]	Mass of JTSIM	Lifetime
Value	<0.1 K	<0.1°	745×488×408	44 kg	8 years

DARA also has three electrical, substitution radiometers (Channel A, Channel B, and Channel C). The difference is that they are aligned in a triangle. Compared to PMO6, DARA inverts the aperture geometry to eliminate stray light. The design of the new cavity and heat sink reduces the non-equivalence.

Table 1 summarizes the instrument parameters of the *Fengyun*-3E/JTSIM.

2.2. The Sensor Box of JTSIM

As can be seen in Figure 3, SIAR has three channels in the Sensor Box, and each channel has two small, inverted cavities inside the cylindrical shield: one is the primary cavity and the other is for reference. The cavities are painted with specular black paint and tied to the heat sink. To reduce the thermal noise of the radiometers, all cavities share the same heat sink. Heating wires are embedded in the walls of the primary cavity using a special chemical method. The insulation ring is laid at the open side of the primary cavity and is surrounded by 145 pairs of thermocouples.

In order to detect the temperature difference between the primary cavity and the heat sink, the hot junctions of the thermocouples are connected to the primary cavity, and the cold junctions are connected to the heat sink. The ring of thermocouples is the same design for the reference cavity. In order to compensate the temperature drift of the heat sink with the external thermal environment, the ring of thermocouples in the primary cavity and the ring of thermocouples in the reference cavity are connected in series.

For the measurement of solar irradiance, the view-limiting apertures, mounted in front of the detector, provide a full field of view of 6°. The precision apertures are mounted in

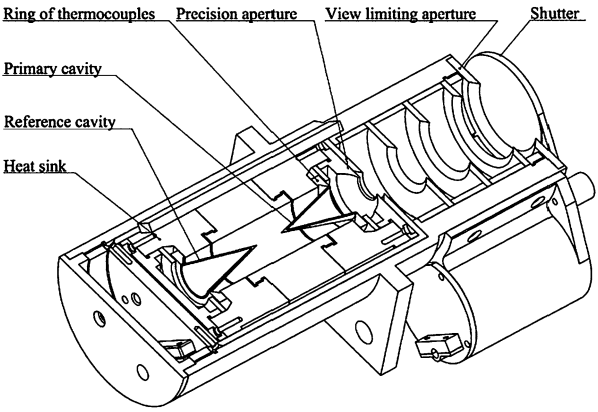

Figure 3 Cavity schematic of SIAR radiometer used in JTSIM. Overall size is 745×488×408 mm.

front of the primary cavities. They have a nominal diameter of 8 mm. Several black baffles are mounted between the view-limiting aperture and the precision aperture to prevent unexpected stray light from entering the primary cavity. When SIAR is working in the calibration phase, the shutter located at the top of the metal cylinder is used to block the solar irradiance.

The DARA detector heads feature three conical cavities. The cavities are made of silver (130 μm), coated with a gold layer (5 μm) on the outside. The cavity is attached to the heat-link aluminum structure using the ultrasonic welding technique. The advantage of this technique is that there is no solder necessary, which would add to the thermal mass of the cavity. The heat sink is made of aluminum (AW 6082) and attached to the front plate. The whole heat-sink and heat-link structure is machined from one solid piece of aluminum. In front of the instrument are the precision apertures. They are fixed to the front plate. The apertures are made of tungsten carbide (RGS 50). They have a nominal diameter of 5 mm. DARA has a slope angle of 1° and a nominal field of view of 3.65°. DARA thus has a limit angle of 6.28°.

2.3. The Electronics Box of JTSIM

The electronics system for JTSIM includes the irradiance-measurement system, the Sun-tracking system, the temperature-control system, and the communication system. The Sun-tracking system includes the Sun sensor, two axis motors, the inner and outer frame, etc. This system provided a good solar pointing for the *Fengyun*-3C/SIM-II, and TSI has been measured daily with it from 1 October 2013 until now. The Sun-pointing error was less than 0.1°. The temperature-control system provided 24 channels of coarse temperature control for the frame and two channels of fine temperature control for the heat sink. The temperature-control accuracy of the heat sink was less than 0.1 K, which keeps the instrument characteristics constant while in orbit. The onboard software of SIAR processes the data and calculates the irradiance values online. All of the raw data are downlinked by the communication system through the 1553B channels of the spacecraft. We can use the raw data for more sophisticated evaluations, corrections, and diagnostics. The raw data for corrections involve the established temperature, the estimation of the current, etc. As can be seen in Figure 4, SIAR irradiance-measurement system operates in two phases.

When SIAR is operated in the measurement phase, the shutter is open, and the primary cavity is heated by the absorption of solar radiation [$P_{\odot}$] and the additional electrical power

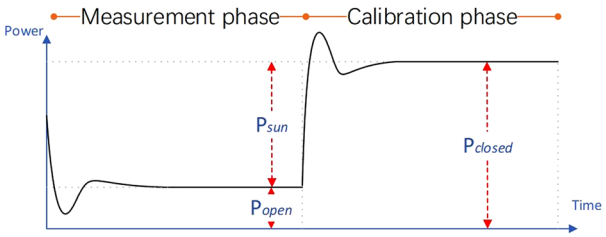

Figure 4 The irradiance-measurement phases.

[P_{open}]. When SIAR is operated in the calibration phase, the shutter is closed, and the primary cavity is only heated by electrical power [P_{closed}]. The radiant power of the Sun is the difference in electrical power between the measurement phase and the calibration phase. This is how the radiant power is determined. The electrical heating-voltage reference is provided by the AD586 precision voltage reference**.** The heating-wire resistance is connected by four wires. Two wires are for the heating, and the others are for the heating-state sampling. This heating method can avoid the influence of the heating wire resistance. The solar radiation can be calculated by Equations 1 – 3:

$$P_{\odot} = P_{\text{closed}} - P_{\text{open}} \tag{1}$$

$$P_{\text{closed}} = \frac{V_{\text{closed}}^2}{R} \tag{2}$$

$$P_{\text{open}} = \frac{V_{\text{open}}^2}{R} \tag{3}$$

Here $P_{\odot}$ denotes the solar-radiation heat power, P_{open} denotes the electrical heat power when the shutter is open, P_{closed} denotes the electrical heat power when the shutter is closed, R denotes the heating-wire resistance, V_{open} denotes the electrical-heat voltage when the shutter is open, and V_{closed} denotes the electrical-heat voltage when the shutter is closed.

In order to compensate for the temperature drift, the reference cavity is supplied with constant power. If the environment temperature changes, the cavity and the heat-sink temperature will drift and influence the measurement. Using an identical cavity as the reference cavity to suppress these effects, the heat flux between the cavity and the heat sink is equal for both cavities.

For DARA, all three cavities can be used as active cavities. However, one of the three cavities is always used as a reference cavity. This means that the instrument can operate with a single active cavity, two active cavities in parallel, or two cavities operating with inverted shutter cycles. This design offers redundancy in case one of the cavities fails. The electronics of DARA consist of a two-channel digital controller loop, a data-acquisition system, and a communication interface. The controller loop is responsible for keeping the active and the reference cavity in thermal balance. Analogue-to-digital converters are used to sample the error signals as well as the voltage on the heaters. These values plus the values of the duty cycle as generated by the controller are continuously logged at a sampling rate of 20 Hz. Housekeeping signals, for example temperatures and pointing sensor data, are read at a lower rate (Wang et al., 2017).

3. The Characterization of JTSIM

In order to measure the solar irradiance in SI units [$\mathrm{W\,m^{-2}}$], all of these components of SIAR, have to be characterized experimentally:

$$\mathrm{TSI} = \frac{\left(P_{\mathrm{Sun}} - P_{\mathrm{Space}}\right)}{A_{\mathrm{p}}} \times f_{\mathrm{diff}} \times f_{\mathrm{absor}} \times f_{\mathrm{non}} \times f_{\mathrm{AU}} \times f_{\mathrm{dopp}}. \tag{4}$$

Here $P_{\odot}$ denotes the solar radiation heat power, P_{space} denotes the radiation from the instrument to the background space, A_{p} denotes the precision-aperture area, f_{diff} denotes the diffraction-losses coefficient, f_{absor} denotes the cavity absorptance coefficient, f_{non} denotes the non-equivalence error coefficient, f_{AU} denotes the Earth–Sun distance coefficient, and f_{dopp} denotes the Doppler-effect coefficient.

3.1. Aperture Area

The TSI unit is $\mathrm{W\,m^{-2}}$, and the area of the aperture defines the $\mathrm{m^2}$ directly. The apertures of SIAR are made of cemented tungsten carbide (RGS 50), and all three apertures have the same design diameter of 8 mm. The aperture-area measurement was carried out on an ultra-precise coordinate measuring machine at the Swiss Federal Office of Metrology (METAS). With three laser interferometers, the position of its displacement table was measured and fitted with a probing head using a very weak probing force of less than 0.5 mN. This machine ensures an accurate measurement without plastic deformation even when using very small size probes. The probe is a sapphire sphere, and the diameter is only 0.3 mm. The edge of the aperture area was probed in a series of 18 circles spaced by 2.5 µm in height. All measurement points were scanned with a point density of about 250 points $\mathrm{mm^{-1}}$. Every 0.2° on the opening circumference, the most inner point from the 18 circles was projected onto the top plane of the aperture. The aperture area delimited by these most inner points was then computed.

The temperature of the port reducer during the measurements was 20 °C ± 0.02 °C. The results were corrected to the reference temperature of 20 °C. The uncertainty of measurement is between 0.0023 $\mathrm{mm^2}$ to 0.0025 $\mathrm{mm^2}$, and it is stated as the combined standard uncertainty multiplied by two, that is the 95% confidence interval. The measurement uncertainty contains contributions originating from the measurement standard, from the calibration method, from the environmental conditions, and from the object being calibrated. The long-term characteristics of the object being calibrated are not included. RGS50 is made of tungsten–carbide and cobalt (15%). Its thermal expansion is similar to metals. The linear expansion coefficient [α] is 6 ± 1 ppm $\mathrm{^{\circ}K^{-1}}$ (Shearer, 2014). The thermal expansion of the aperture area results in 12 ppm per Kelvin. The aperture temperature of SIAR in orbit is about 25 °C ± 10 °C. Therefore, the uncertainty for the aperture-area temperature-correction factor [$c_{\alpha}(T)$] is a function of T with a maximum of 31 ppm ($k = 1$). The combined uncertainty is 55 – 59 ppm. Table 2 summarizes the aperture-area measurement results.

3.2. Cavity Absorptance

The ideal cavity should absorb all incoming radiation from the Sun. In reality, there is no ideal absorber material. In order to correct the TSI measurement of SIAR, the absorption correction had to be determined by experiment. In order to achieve a high absorptivity, the cavity of SIAR has a conical shape. SIAR's three cavities are painted with a special black paint to achieve matte and absolutely diffuse surfaces.

Table 2 Aperture area measurement results of the Solar Irradiance Absolute Radiometer (SIAR).

	Measured area [mm^2]	Area uncertainty [ppm]	Temperature uncertainty [ppm]	Combined uncertainty [ppm]
Channel 1	50.2530	46	31	55
Channel 2	50.2591	50	31	59
Channel 3	50.2667	46	31	55

First, we used a spectrophotometer to measure the reflectivity of the black paint, which is defined as η_λ. As can be seen in Figure 5, the wavelength measurement covers from 200 nm to 20 μm. The uncertainty for the black-paint reflectivity measurement is 1% ($k = 2$). Second, each cavity of SIAR was scanned with a 633 nm laser beam (HNL210L-EC). The laser scan covered an area of 5.0 × 5.0 mm^2 with a resolution of 0.2 mm. The optical source was entering the integrating sphere vertically and then reflected by a sample. Meanwhile the silicon-photodiode outputs a response voltage. Xiaolong Yi's work provides a method for measuring the conical cavity absorptance [α_λ] with the integrating sphere and the digital two-dimensional platform (Yi et al., 2016), which is the substitution method. The 633 nm laser beam entered the integrating sphere vertically and was reflected. The response voltage was produced by the silicon photodiode. The experiment had three steps: First, the conical cavity [ρ_C] was placed in the sample region, and the response voltage is U_C. Second, the conical cavity was substituted by the standard white board, whose reflectivity [ρ_S] was calibrated. The response voltage is U_S. Finally, the standard white board was taken from the sample region. Therefore, the optical source passed through the integrating sphere. The response voltage of background is U_B. Figure 5 shows the absorptance map of the cavity. We can calculate the cavity absorptance rate of 633 nm [α_{633}] by Equation 5:

$$\alpha_{633} = 1 - \frac{U_c/u_c - U_B/u_B}{U_S/u_S - U_B/u_B} \times \rho_S. \tag{5}$$

During the experiment, the optical power of the laser may change, which reduces the measurement accuracy. Therefore, we needed the reference optical path to monitor the optical source during the measurement process. In the spectrophotometer measurement, the laser was reflected only once by the black paint. In the cavity-absorptance measurement, we defined the equivalent number of reflections [N], which meant the laser beam would need N reflections to back-reflect out of the cavity. We can calculate N by Equation 6:

$$N = \frac{\log(1 - \alpha_{633})}{\eta_{633}}. \tag{6}$$

With N, we can calculate from 200 nm to 20 μm with Equation 7:

$$\alpha_\lambda = 1 - \eta^N \tag{7}$$

In order to obtain a correction that is applicable for measurements of solar irradiance, the measurements were weighted with a solar spectrum. As can be seen in Figure 5, the solar-weighted reflectance is less than 0.1%. The absorptances of all three cavities are over 99.9%. The combined uncertainty is 7 – 17 ppm. Table 3 summarizes the cavity-absorptance measurement results.

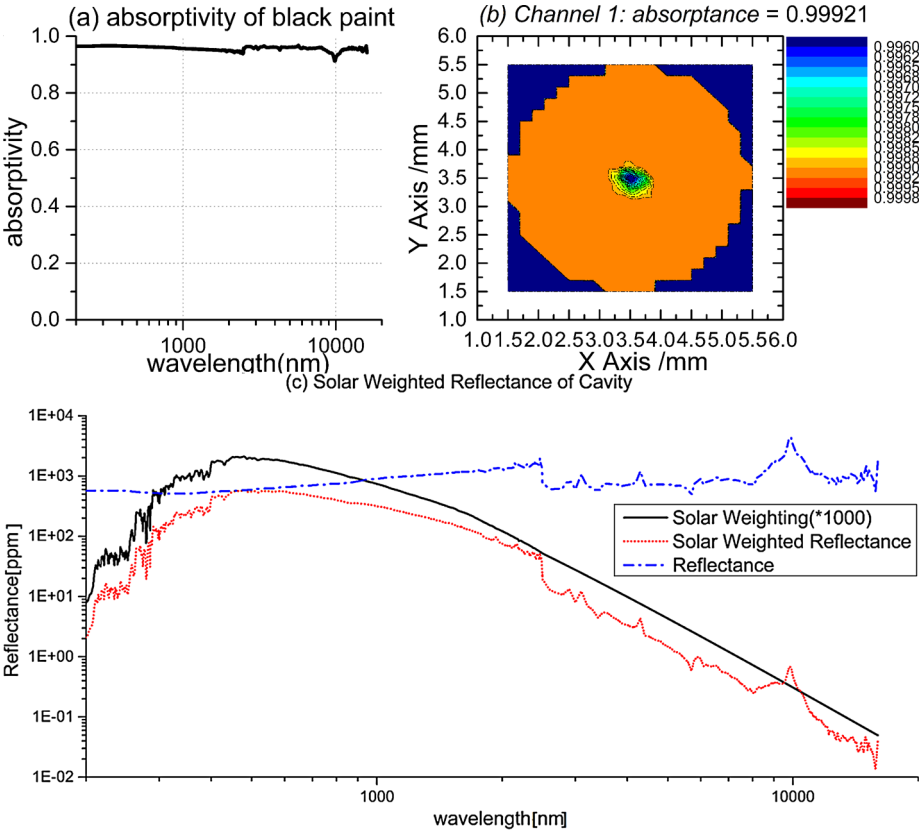

Figure 5 The cavity-absorptance measurement result of SIAR: (**a**) reflectivity of the black paint; (**b**) absorptance map of the cavity; (**c**) solar-weighted reflectance of the cavity.

3.3. Non-equivalence

The non-equivalence effect is caused by the slight heat-flow difference in the thermal configuration of the active cavity in the measurement and calibration phases. Take PMO6 for example; the non-equivalence is explained by a spurious heat flow through the air from the cylindrical part of the cavity to the radiation shield (Brusa and Fröhlich, 1986). So, the non-equivalence of PMO6-type radiometers cannot be negligible. DARA and SIAR-type radiometers are different from the PMO6-type radiometer. The cone is inverted and the radiation shields are placed further apart from the critical parts of the cavity. A slight misplacement of the heater element can cause a difference in the temperature distribution. Considering this, the wires of SIAR were embedded into the walls of the primary cavity using a special chemical method, and one insulation ring surrounded by 145 pairs of thermocouples is placed at the open side of the primary cavity (Wang, Li, and Fang, 2014; Tang et al., 2016). Therefore, the exact position of the heater element is crucial to reduce the non-equivalence effect. As the cavity is essentially hand crafted, it is expected to be slightly imperfect. The influence of heat flow at ambient pressure is different from in a vacuum. Walter et al. (2017) did a simple model calculation. The result showed that for CLARA-type radiometers the non-equivalence effect is about 7±4 ppm in vacuum conditions. We used

Table 3 The cavity absorptance measurement result of SIAR. Type A uncertainty is measurement repeatability; Type B uncertainty is from the reference instrument, the influence of the measurement environment, and the approximations of the measurement methods.

Parameter	Channel 1		Channel 2		Channel 3	
	Value	σ_{A+B} [ppm]	Value	σ_{A+B} [ppm]	Value	σ_{A+B} [ppm]
U_c	0.0088	37.0+4	0.0089	37.0+4	0.0090	37.0+4
u_c	2.8062	242.6+70	2.8062	256.9+70	2.8062	256.9+70
U_s	6.1094	1070.7+70	6.0768	1507.6+70	6.1090	1507.6+70
u_s	2.8068	335.7+70	2.8065	307.5+70	2.8068	307.5+70
U_B	0.0047	103.9+4	0.0046	17.1+4	0.0047	17.1+4
u_B	2.8064	226.4+70	2.8064	270.5+70	2.8064	270.5
α_{633}	0.99934	17.5+60	0.99933	7.3+60	0.99932	7.2+60
η_λ	<0.05	100.0+44	<0.05	100.0+44	<0.05	100.0+44
$\alpha_{\lambda(\text{solar weighted})}$	0.999214		0.999210		0.999197	
Uncertainty (A+B)	126		125		125	

the same model to calculate SIAR, and the uncertainty was more or less close to CLARA. For operation in space applications, non-equivalence is considered negligible as justified in the model approach. However, for the calibration with the WRR standard in ambient air, the influence of heat flow cannot be ignored.

To determine the air-to-vacuum ratio before launch, SIAR was placed in a vacuum chamber that is mounted on the solar tracker. There is a window on the vacuum chamber, which was placed in front of the SIAR apertures. The window is inclined by 4° to avoid backscatter from the front plate via the window into the cavity. A PMO6-type radiometer was mounted next to the vacuum chamber as the reference instrument. SIAR was first operated in vacuum for three hours, then the vacuum chamber was filled with nitrogen to ambient pressure. After half an hour, the instrument was in acceptable thermal equilibrium. Then TSI data could be taken without being influenced by large thermal drifts. For the next 1.5 hours, the instrument was operated in ambient pressure conditions until the Sun was out of view. SIAR was operated with a 60-second shutter cycle. The measurements were performed on 24 June 2019 – 28 June 2019 at the PMOD/WRC lab. As can be seen in Figure 6, the PMO6 reference instrument is without a window, so the ratio of SIAR with a window to PMO6 is 0.93 – 0.94. As can be seen in Figure 7, the air-to-vacuum ratios determined by single-sequence fits are over 0.995. Considering the losses due to window reflections and the dust accumulation on the windows during the experiment, different adjustments to improve the measurement were made. The resulting correction factors for the non-equivalence of SIAR are listed in Table 4.

3.4. Diffraction

Because electromagnetic radiation propagates as a wave, the radiation does not exactly follow the path one would assume from purely geometrical optics. The wave nature of the radiation creates diffraction effects at the front aperture of the SIAR instrument. This reduces the amount of power reaching the detector, compared to what is expected by geometrical optics. Therefore, we needed to calculate the diffraction effect: the influence of the solar

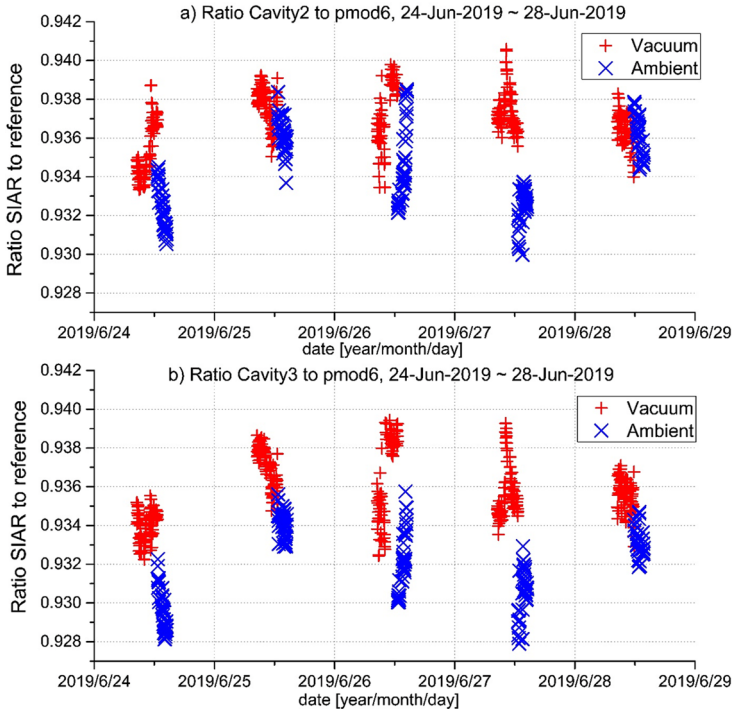

Figure 6 Ratio of SIAR with window to the PMO6 reference instrument without window: (**a**) cavity 2, (**b**) cavity 3.

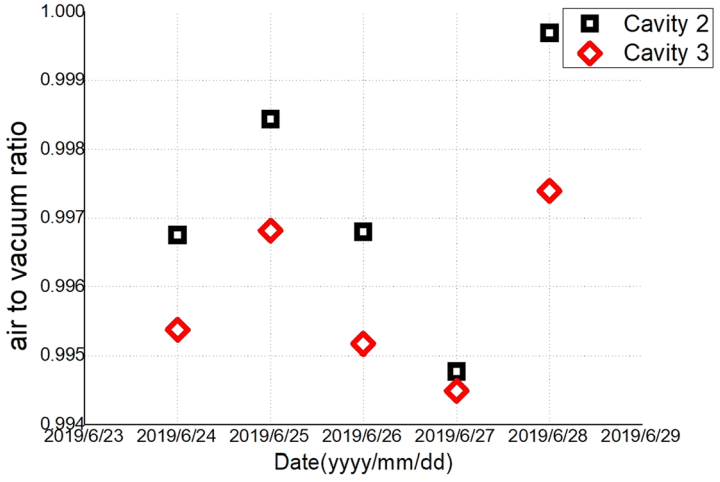

Figure 7 Overview of the air-to-vacuum ratios determined by single-sequence fits.

spectrum on the diffraction correction. Shirley has contributed many articles on diffraction effects in radiometry (Shirley and Eric, 1998; Shirley, 2005), which were the basis for the diffraction-correction calculation of SIAR. Table 5 shows the diameters of all apertures and

Table 4 The resulting correction factors for the non-equivalence of SIAR (in ambient).

Channel	Channel 1	Channel 2	Channel 3
Number of measurements per day[a]	90+40	90+40	90+40
Number of measurement days	5	5	5
Correction factor (in ambient)	0.9333±131 ppm	0.9342±129 ppm	0.9318±132ppm
Correction factor (in vacuum)	0.9361±116 ppm	0.9369±118 ppm	0.9358±112ppm
air-to-vacuum ratio (no correction)	0.997009	0.997295	0.995787
Loss due to window reflections	39 ppm	39 ppm	39 ppm
air-to-vacuum ratio (after correction)	0.996970	0.997256	0.995748
Non-equivalence (after correction)	1.00304	1.00275	1.00427
Combined uncertainty 1σ	175 ppm	175 ppm	173 ppm

[a]Vacuum conditions + ambient conditions.

Table 5 The diameters of all apertures in SIAR and the distance between them.

	View limiting aperture	Baffle 1	Baffle 2	Baffle 3	Baffle 4	Precision aperture
Diameter [mm]	13.24	12.2	11.14	10.1	9.04	8
Distance [mm]	20	20	20	20	20	

the distance between them. The diffraction correction after calculation is 1.00164 and the uncertainty is 50 ppm.

3.5. Summary

Some important experiments related to the characterization of SIAR have been discussed above. The heating resistance of SIAR is connected by four wires. During the measurement, the cavity of SIAR was directly heated by the standard voltage source, so the correction factor was the heater resistance and the voltage-standard reference. The heater resistance and the voltage standard were measured by Fluke 8508A at the CIOMP laboratory. Table 6 summarizes all of the correction factors and the combined uncertainties resulting from the characterization of SIAR and DARA. The characterization data of DARA are supported by PMOD/WRC. Some characterization data of the TIM are from Kopp, Heuerman, and Lawrence (2005) and Kopp, Lawrence, and Rottman (2005).

4. Calibration of the JTSIM Instrument

4.1. Calibration Set-up at Lijiang

In order to have accurate and consistent scientific data on orbit, it is important to characterize and calibrate JTSIM carefully before launch, as well as having an overlap between the measurement periods of DARA and SIAR. As can be seen in Section 2, the important parameters of SIAR and DARA were measured or calculated. The characterization is at the component-level calibration of all parameters of SIAR in the lab. The measured result of all

Table 6 Summary of the JTSIM characterization corrections for measurements of solar irradiance (in ambient).

Native scale	SIAR						DARA						TIM
	Channel 1		Channel 2		Channel 3		Channel A		Channel B		Channel C		
Item	value	σ [ppm]	value	σ [ppm]	value	σ [ppm]	value	σ [ppm]	value	σ [ppm]	value	σ [ppm]	σ [ppm]
Aperture area [mm^2]	50.2530	46	50.2591	50	50.2667	46	19.6140	42	19.6144	49	19.6172	40	55
Aperture temp.	–	39	–	39	–	39	–	39	–	39	–	39	–
Cavity absorptivity	0.99921	126	0.99921	125	0.99920	125	0.99897	160	0.99906	160	0.99900	160	54
Diffraction	1.00164	50	1.00164	50	1.00164	50	1.00122	43	1.00122	43	1.00122	43	–
Non-equivalence	1.00304	175	1.00275	175	1.00427	173	1.00040	85	1.00087	66	1.00044	70	–
leading heat	–	–	–	–	–	–	1.00050	25	1.00064	25	1.00052	25	–
Readout electronics	–	30	–	30	–	30		70	–	70	–	70	–
Heater resistance [Ω]	862.163	17	861.543	17	860.777	17	–	0	–	0	–	0	17
voltage standard [V^2]	25.0118	16	25.0118	16	25.0118	16	–	–	–	–	–	-	7
Total calibration factor	1.005479		1.005189		1.006722		1.003154		1.003675		1.003185		
Combined uncertainty [ppm]	233		233		231		205		199		199		

Table 7 The International Pyrheliometer Comparison (IPC-XII) report in 2015.

	WRR factor	Σ [ppm]	Number
PMO6-LINARD	1.020799	465	563
PMO6-CC	1.000335	522	542
SIAR-2C	0.998949	753	392

parameters can be traceable to the International System of Units (SI). An end-to-end calibration is a procedure where JTSIM is directly calibrated with the WRR reference radiometers. The WRR scale is the reference scale of World Meteorological Organization (WMO), which is officially used in meteorological measurements of solar radiation. The three reference radiometers for the calibration are the PMO6-CC, PMO6-LINARD, and SIAR-2C. These reference radiometers participated in the International Pyrheliometer Comparison (IPC-XII) in 2015. During IPC-XII, they were compared against the World Standard Group (WSG) at PMOD (Finsterle, 2016). The WSG represents the WRR standard for solar-irradiance measurements. The WRR Factor from the IPC-XII report can be seen in Table 7. The WRR is made up of the corrected data from all three reference radiometers.

The calibration of JTSIM was performed at the Lijiang Observatory, which is suitable for irradiance measurements due to the clear sky and good view of the Sun. The PMO6-CC and PMO6-LINARD were mounted on one Sun tracker, which can point to the Sun for the whole day. The pointing error is less than 0.1°. SIAR-2C and JTSIM were also mounted on the other Sun tracker. They measured the solar irradiance side by side. The rules for calibration are as follows. First, set SIAR to the reference phase of 60 seconds and the measurement phase of 60 seconds. Then synchronize SIAR with the reference instruments to ensure the shutters close at the same time. The calibration is separated into several series, and the instrument produces 13 group values of the solar irradiance per series. It ran for three days, from 05 December 2019 to 07 December 2019, and each full day of observations was performed with all three cavities of SIAR. The raw data of the SIAR calibration on 07 December 2019 can be seen in Figure 8.

4.2. Data Evaluation and Results from the Calibration

Figure 9 shows the irradiance data and the corresponding ratios for theSIAR to WRR from 05 December 2019 to 07 December 2019. The number of measured data points is over 580. Several corrections were applied to these data. First, we must consider the influence of the ambient temperature. As a result of the change in the ambient temperature during the measurement period, the heating-wire resistance, the reference-voltage standard, and the area of the apertures all needed a temperature correction. The heating-wire resistance is made of constantan, and the temperature coefficient of resistance is 30 ppm K^{-1}. The precision voltage is produced by AD586, which is the high-precision 5 V reference, and the temperature-drift coefficient for AD586 (Grade B) is 5 ppm K^{-1}. The precision apertures of SIAR are made of cemented tungsten carbide (RGS 50), and the thermal expansion coefficient is 6 ppm K^{-1}. Because the exact temperature for the temperature correction is not known, we could only use the instrument-temperature data in the housekeeping data and the environment temperature data from the meteorological station at the Lijiang Observatory.

For the data evaluation of the SIAR calibration, the absorptance factor, the tracking error factor, the diffraction correction, and the air-to-vacuum ratio were not applied to these data. After the data evaluation, the weighted ratios to WRR for the three cavities of SIAR are 0.99939, 1.00092, and 0.99965. The data consistency between the three cavities and WRR is better than 0.1%.

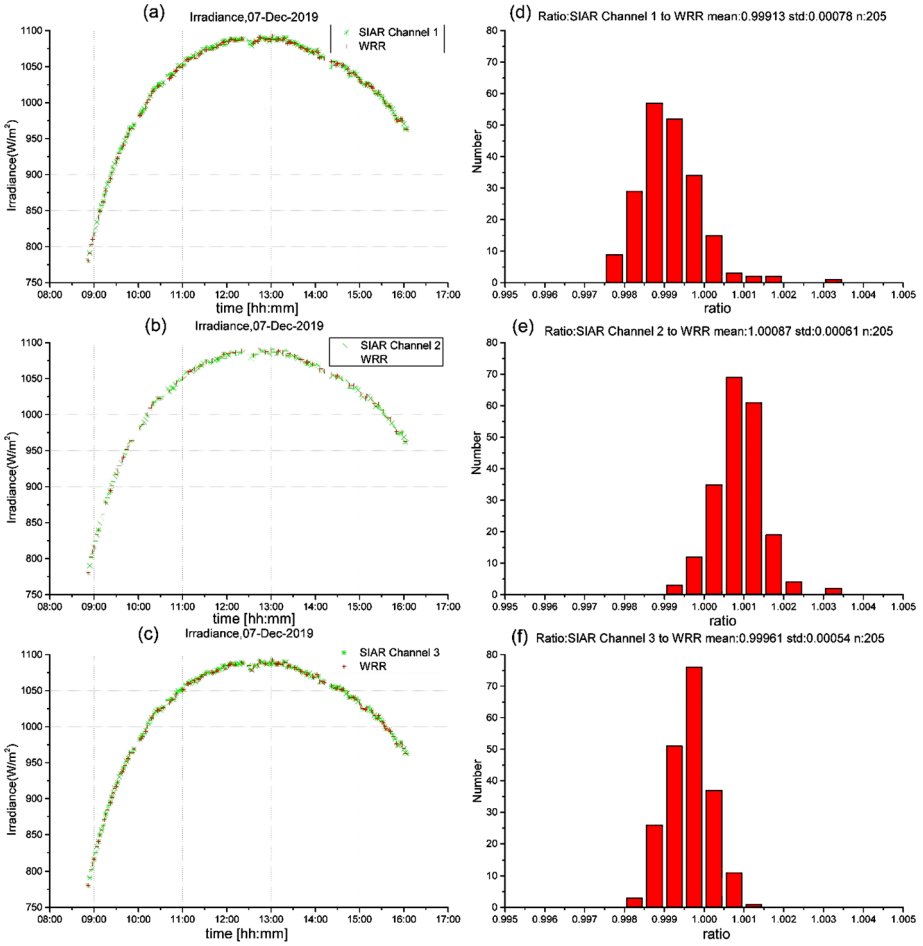

Figure 8 The SIAR Calibration Raw Data (7 December 2019): (**a**) cavity 1 irradiance; (**b**) cavity 2 irradiance; (**c**) cavity 3 irradiance; (**d**) cavity 1 corresponding histograms; (**e**) cavity 2 corresponding histograms; (**f**) cavity 3 corresponding histograms.

4.3. Uncertainties of the Calibration

Table 7 lists the ratio of SIAR to WRR for each measurement day. For the uncertainties of SIAR, we needed to consider the measurement statistical uncertainty (Type A) and the system calibration uncertainty (Type B). The statistical uncertainty of the ratio measurement is from the measured data of the three days of calibration, which is listed in Table 8. The system uncertainty of the calibration is associated with the three WSG reference instruments. We considered the aspects such as how accurate a representation is the reference radiometer for the WRR, the uncertainty of the WSG data acquisition, and the thermal expansion of the aperture. The corresponding standard-uncertainty value is given by the WRC calibration procedures, and it is also listed in Table 8. The combined uncertainties for the three cavities of SIAR are 0.099%, 0.076%, and 0.074%. In other words, the calibration accuracy for the three cavities of SIAR is better than 0.1%. Table 9 summarizes the calibration factor

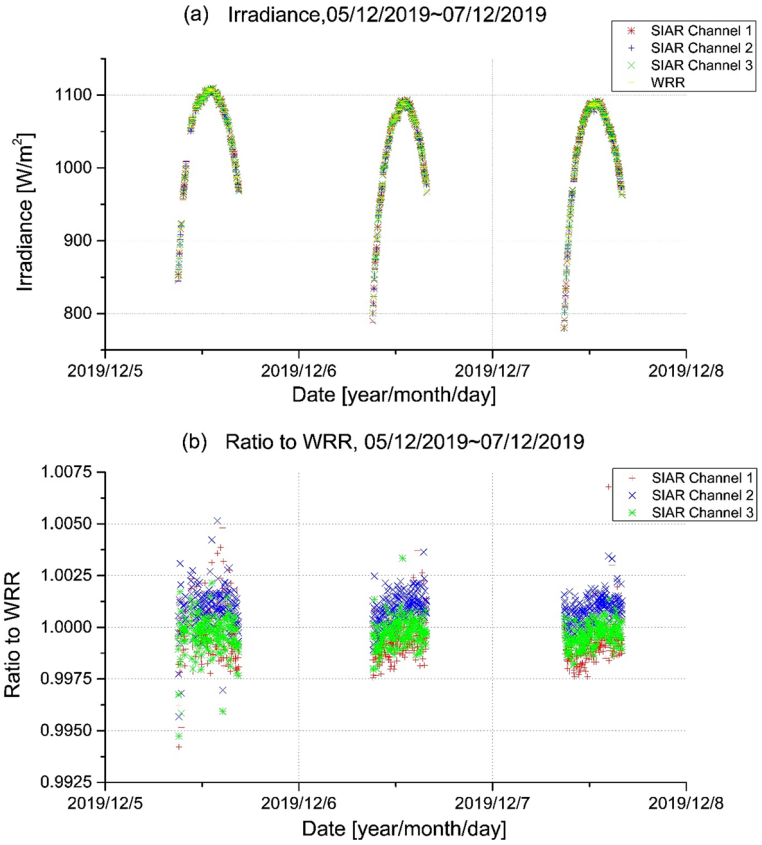

Figure 9 SIAR Calibration Data (5 December, 6 December, 7 December 2019): (**a**) irradiance; (**b**) ratio to WRR.

Table 8 Ratio of SIAR to World Radiometric Reference (WRR) (Raw Data, with only circumsolar correction applied).

Date	N_{meas}	T_{mean}	Channel 1	Channel 2	Channel 3
5-Dec	181	3.0 °C	0.99968±0.00124	1.00097±0.00080	0.99968±0.00080
6-Dec	194	3.3 °C	0.99923±0.00071	1.00095±0.00064	0.99970±0.00061
7-Dec	205	4.0 °C	0.99913±0.00078	1.00087±0.00061	0.99961±0.00054
Weighted mean of ratio			0.99939	1.00092	0.99965
Statistical uncertainty			0.00093 (3σ)	0.00068 (3σ)	0.00065 (3σ)
Calibration uncertainty			0.00035	0.00035	0.00035
Total Uncertainty			0.00099	0.00076	0.00077

and the combined uncertainties of DARA and SIAR. DARA was successfully developed by PMOD/WRC, and the DARA calibration data were provided by PMOD/WRC.

Table 9 The calibration factor and the combined uncertainties of the *Digital Absolute Radiometer* (DARA) and SIAR.

	SIAR			DARA		
	Channel 1	Channel 2	Channel 3	Channel A	Channel B	Channel C
Ratio to WRR	0.99939	1.00092	0.99965	0.99390	0.99317	0.99381
Uncertainty (3σ)	0.0010	0.0008	0.0007	0.0004	0.0004	0.0004

5. Conclusion

In this article, we introduce the new generation of light-weight radiometers (JTSIM) for space applications developed and built by CIOMP/CAS and PMOD/WRC. The *Fengyun*-3E/JTSIM is the first example of international cooperation for TSI measurement on a *Fengyun*-series spacecraft. DARA from PMOD and SIAR from China will measure the solar irradiance at the same time for eight years. We describe the electronics box and the sensor box of JTSIM, the characterization, and the calibration results. The characterization factor of SIAR includes the aperture area, the cavity absorptance, the non-equivalence, the diffraction, etc. We summarize all of the correction factors and the combined uncertainties resulting from the characterization of SIAR: the combined correction factor is 1.0051 – 1.0067, and combined uncertainty is 231 – 233 ppm. As can be seen in Table 6, compared to DARA, the non-equivalence experiment may be the main reason for this, as a result of the insufficient number of sunny days at PMOD/WRC during the limited SIAR-testing phase.

The weighted ratio to WRR for the three cavities of SIAR is 0.99939 – 1.00092. The data consistency between the three cavities and WRR is better than 0.1. The combined uncertainty for the three cavities of SIAR is 0.074% – 0.099%. The SI radiant power scale, however, is directly traceable to basic SI units. It is realized with cryogenic laboratory radiometers. As a result of the schedule for launch, SIAR cannot be compared to the SI calibration at the TRF. However, as can be seen in Table 6, the calibration results of DARA and SIAR compared against WRR are in very good agreement. The fourth WRR to SI comparison yielded a 0.31% difference between these two scales by PMOD/WRC (Fehlmann et al., 2012). Therefore, the SI calibration factor of SIAR can be calculated, and the calibration result will ultimately be applied to the space-borne JTSIM TSI measurements onboard the *Fengyun*-3E spacecraft.

Acknowledgments This work is sponsored by the *Fengyun*-3 Chinese Space Program and supported by Chinese Meteorological Administration (CMA) and Swiss Space Center. The authors would like to thank numerous staff members at PMOD/WRC, who gave great support for the aperture-area manufacture, the non-equivalence experiment, the WRR calibration, etc. The authors also thank the staff at Federal Institute of Metrology (METAS) for the aperture-area measurement. This work was also supported by the National Key R&D Program of China under grant (No. 2018YFB0504600, No. 2018YFB0504603).

Disclosure of Potential Conflicts of Interest The authors declare that they have no conflicts of interest.

Publisher's Note Springer Nature remains neutral with regard to jurisdictional claims in published maps and institutional affiliations.

References

Brusa, R.W., Fröhlich, C.: 1986, Absolute radiometers (PMO6) and their experimental characterization. *Appl. Opt.* **25**, 4173. DOI.

Butler, J.J., Johnson, B.C., Rice, J.P., Shirley, E.L., Barnes, R.A.: 2008, Sources of differences in on-orbital total solar irradiance measurements and description of a proposed laboratory intercomparison. *J. Res. Natl. Inst. Stand. Technol.* **113**, 187. DOI.

Fang, W.: 2003, Solar irradiance absolute radiometer and international comparison. *Acta Opt. Sin.* **23**, 112. DOI.

Fang, W., Yu, B., Wang, Y., Gong, C., Yang, D., Ye, X.: 2009, Solar irradiance absolute radiometers and solar irradiance measurement on spacecraft. *Chin. J. Opt. Appl. Opt.* **02**, 23. DOI.

Fehlmann, A., Kopp, G., Schmutz, W., Winkler, R., Finsterle, W., Fox, N.: 2012, Fourth World Radiometric Reference to SI radiometric scale comparison and implications for on-orbit measurements of the total solar irradiance. *Metrologia* **49**, 34. DOI.

Finsterle, W.: 2016, International Pyrheliometer Comparison (IPC-XII) final report. *WMO IOM Rep.* **124**, 179. URL: https://library.wmo.int/index.php?lvl=notice_display&id=19643#.YEXogaEw89t.

Kopp, G., Lean, J.L.: 2011, A new, lower value of total solar irradiance: evidence and climate significance. *Geophys. Res. Lett.* **38**, 112. DOI.

Kopp, G., Heuerman, K., Lawrence, G.: 2005, The Total Irradiance Monitor (TIM): instrument calibration. *Solar Phys.* **230**, 111. DOI.

Kopp, G., Lawrence, G., Rottman, G.: 2005, The Total Irradiance Monitor (TIM): science results. *Solar Phys.* **230**, 129. DOI.

Schmutz, W., Fehlmann, A., Finsterle, W., Kopp, G., Thuillier, G.: 2013, Total solar irradiance measurements with PREMOS/PICARD. In: Cahalan, R.F., Fischer, J. (eds.) *Radiation Processes in the Atmosphere and Ocean (IRS2012): Proc. Internat. Radiation Symp. (IRC/IAMAS)* **CP-1531**, AIP, Melville, 624. DOI.

Shearer, T.R.: 2014, The Designer's Guide to Tungsten Carbide. General Carbide. Accessed 3 July 2020. URL: www.generalcarbide.com/PDF/Designer-Guide.pdf.

Shirley, E.L.: 2005, Diffraction effects in radiometry. *Exp. Methods Phys. Sci.* **41**, 409. DOI.

Shirley, E.L., Eric, L.: 1998, Revised formulas for diffraction effects with point and extended sources. *Appl. Opt.* **37**, 6581. DOI.

Tang, X., Fang, W., Wang, Y., Yang, D., Yi, X.: 2016, Time constant optimization of solar irradiance absolute radiometer. *Optoelect. Lett.* **13**, 179. DOI.

Thuillier, G., Dewitte, S., Schmutz, W.: 2006, Simultaneous measurement of the total solar irradiance and solar diameter by the PICARD mission. *Adv. Space Res.* **38**, 1792. DOI.

Walter, B., Levesque, P.L., Kopp, G., Andersen, B., Beck, I., Finsterle, W., Gyo, M., Heuerman, K., Koller, S., Mingard, N.: 2017, The CLARA/NORSAT-1 solar absolute radiometer: instrument design, characterization and calibration. *Metrologia* **54**, 674. DOI.

Wang, H., Li, H., Fang, W.: 2014, Timing parameter optimization for comparison experiments of TSIM. *Appl. Opt.* **53**, 1718. DOI.

Wang, Y., Fang, W., Gong, C., Yu, B.: 2007, Dual cavity inter-compensating absolute radiometer. *Opt. Precis. Eng.* **15**, 1662. DOI.

Wang, H., Wang, Y., Ye, X., Yang, D., Wang, K., Li, H., Fang, W.: 2017, Instrument description: the total solar irradiance monitor on the FY-3C satellite, an instrument with a pointing system. *Solar Phys.* **292**, 112. DOI.

Yang, Z., Lu, N., Shi, J., Zhang, P., Yang, J.: 2013, Overview of FY-3 payload and ground application system. *Adv. Meteorol. Sci. Tech.* **50**, 4846. DOI.

Yeo, K.L., Krivova, N.A., Solanki, S.K.: 2014, Solar cycle variation in solar irradiance. *Space Sci. Rev.* **186**, 137. DOI.

Yi, X., Xia, Z., Luo, Y., Fang, W., Wang, Y.: 2016, Correction of cavity absorptance measure method for cryogenic radiometer. *IET Sci. Meas. Technol.* **10**, 564. DOI.

Zacharias, P.: 2014, An independent review of existing total solar irradiance records. *Surv. Geophys.* **35**, 897. DOI.